RSC Applied Polymers

ROYAL SOCIETY OF CHEMISTRY

PAPER

View Article Online
View Journal

Cite this: DOI: 10.1039/d6lp00011h

Multifunctional ion-conductive hydrogels with self-healing, antifreeze, and water-retention capabilities for robust wearable sensing

Zhongyuan Lin, [a] Ze Li,[b] Xinpeng Lv,[b] Yuhang Shen,[a] Chunpeng Ai*[a] and Peng Li*[b]

Conductive hydrogels have attracted attention in the field of wearable electronics due to their softness, biocompatibility, and ionic conductivity. However, challenges such as poor signal stability, limited environmental tolerance, and mechanical fragility hinder broader applications. Here, we report a multifunctional ionically conductive hydrogel (Li-gel) synthesized *via* a two-step process, featuring a polyvinyl alcohol/polyacrylamide (PVA/PAAm) dual network crosslinked with dynamic boronate ester bonds and doped with lithium chloride (LiCl). The hydrogel demonstrates self-healing capability under ambient conditions, and its mechanical strength can recover up to 80% of the original value. It achieves high ionic conductivity (1.1 S m^{-1}) through LiCl-mediated ion transport. LiCl also depresses the freezing point to −13.5 °C and enhances water retention, enabling over 90% mass retention after thermal dehydration and strong resistance to ambient water evaporation. Li-gel exhibits excellent transparency (>90%) and adheres firmly to skin, glass, and plastic, which ensures robust interface stability. Strain-sensing tests yield a gauge factor of 2.00 at 100% strain, with rapid response speed, good strain rate adaptability, and high durability over 1000 stretching–releasing cycles. Altogether, Li-gel combines mechanical resilience, environmental adaptability, and reliable strain-sensing performance, providing a simple and multifunctional hydrogel design for wearable sensing applications.

Received 15th January 2026,
Accepted 24th March 2026

DOI: 10.1039/d6lp00011h

rsc.li/rscapplpolym

1. Introduction

Conductive hydrogels have attracted considerable attention because of the growing demand for biomedical monitoring, intelligent sensing, and human–machine interaction.[1–3] Their unique combination of soft, water-rich elasticity and solid-like mechanical support makes them especially suitable for wearable electronic devices.[4–6] More importantly, conductive hydrogels can effectively transduce multidimensional deformations, such as stretching, bending, and swelling, into real-time electrical signals, providing crucial material support for the development of next-generation soft sensing platforms. Initial strategies for constructing percolated conductive pathways usually involve filler-based approaches to enable either electronic or ionic charge transport. Representative conductive fillers such as carbon nanotubes, graphene, conductive polymers, and silver nanowires have been widely integrated into hydrogel matrices to develop multifunctional sensing systems with continuous conductive networks.[7] For example, Peng *et al.* incorporated PEDOT:PSS into a PVA/PAA dual-network hydrogel to fabricate a multifunctional strain sensor with excellent stretchability, compressibility, and self-adhesive properties, enabling reliable monitoring of complex human motion and broadening the applications of flexible electronics.[8] However, these filler-based conductive hydrogels often suffer from poor stability under large deformations or prolonged cyclic loading, leading to signal drift, insufficient sensitivity, and mechanical fragility.

In addition, the inherently high water content, while enabling softness and signal responsiveness, also exposes hydrogels to issues such as dehydration and freezing.[9] In high-temperature or low-humidity environments, water evaporation can degrade conductivity and irreversibly collapse the network structure; under subzero conditions, ice crystallization and phase transitions can induce brittleness and disrupt ion transport, severely compromising reliability. To overcome these limitations, researchers have explored strategies such as incorporating polyol-based antifreeze agents (*e.g.*, glycerol, ethylene glycol) or hydrophilic natural/synthetic polysaccharides to enhance moisture retention and freeze resistance.[10] However, these approaches often introduce trade-offs, compromising electrical or mechanical performance. Therefore, there is a

[a]*Heilongjiang Provincial Key Laboratory of Micro-nano Sensitive Devices and Systems, Heilongjiang University, Harbin 150080, China.*
E-mail: aichunpeng@hlju.edu.cn
[b]*College of Physical Science and Technology, Heilongjiang University, Harbin, 150080, China. E-mail: lipenghit@hlju.edu.cn*

significant demand for high-performance conductive hydrogels that can maintain stable electrical performance under mechanical strain and exhibit strong environmental adaptability. In contrast, the use of inorganic salts such as LiCl offers dual functionality by promoting ionic conductivity and suppressing ice formation, thereby enhancing environmental resilience without sacrificing mechanical strength or sensitivity.[11,12]

Specifically, in addition to conductivity and environmental stability, the self-healing capability of the hydrogel network has become a key performance criterion for conductive hydrogels intended for long-term operation. Most conventional systems suffer from irreversible structural damage and signal degradation under repeated high-strain loading due to the absence of self-repair mechanisms.[13] This greatly limits their viability in wearable electronics and dynamic strain sensing. To address this issue, recent efforts have focused on designing hydrogels with rapid and reversible self-healing capabilities. For example, He *et al.* reported a triblock copolymer-based hydrogel featuring cation–π interactions, which demonstrated excellent self-healing efficiency and tissue adhesion *in vivo*.[14] However, self-healing conductive hydrogels often rely on dynamic reversible bonds to form weakly crosslinked networks. While these networks enable damage repair, they also reduce mechanical robustness and sensing stability. Under high-precision sensing conditions, such dynamic structures can result in reduced rebound efficiency, delayed signal recovery, and poor microstrain resolution. Moreover, self-healing behavior is often sensitive to external factors such as temperature, humidity, and pH, making it difficult to achieve fast, repeatable repair under variable environments.[15,16] Therefore, achieving a synergistic balance between conductivity, mechanical strength, self-healing, and environmental adaptability remains a core scientific and engineering challenge for next-generation self-healing conductive hydrogels.

To address the coupled requirements of mechanical stability, environmental tolerance, and sensing reliability in flexible conductive hydrogels, this work develops a multifunctional ionic conductive hydrogel (Li-gel) with integrated self-healing, anti-freezing, and water-retention properties. Based on a PVA/PAAm dual-network framework, the hydrogel combines dynamic boronate-ester crosslinking for structural reconfiguration with LiCl-regulated ionic conduction and moisture retention. Rather than introducing entirely unprecedented individual components, the significance of this design lies in the synergistic integration of multiple sensing-relevant functions within a simple aqueous system. The resulting hydrogel exhibits good stretchability, stable ionic conductivity, and preserved functionality under dehydration, elevated temperature, and subzero conditions. In addition, Li-gel shows high transparency and broad interfacial adhesion, which are beneficial for wearable sensing. Practical demonstrations further show that the hydrogel can be used for joint motion monitoring and motion-triggered LED control, indicating its applicability as a multifunctional material platform for wearable strain sensing under mechanically and environmentally variable conditions.

2. Results and discussion

2.1. Cross-linked network and fabrication of hydrogels

PVA, a water-soluble synthetic polymer, has been widely utilized in hydrogel fabrication due to its excellent biocompatibility, film-forming ability, and mechanical flexibility. In the presence of borax ($Na_2B_4O_7{\cdot}10H_2O$), dynamic boronate–diol complexation can occur between adjacent PVA chains, forming reversible borate ester linkages that endow the hydrogel with self-healing and reconfigurable properties. In this study, a dual-network hydrogel based on PVA and PAAm was fabricated *via* a two-step process (Fig. 1a). The first network was physically crosslinked through interactions between PVA and borax, while the second network consisted of chemically crosslinked PAAm.

A mixture containing 1 g of PVA, 1 g of PAAm, 1 g of LiCl, and 0.01 g of *N*,*N*′-methylenebisacrylamide (MBA) was dissolved in 5 mL of deionized water under magnetic stirring at 95 °C for 2 hours. After complete dissolution, 2 mL of an aqueous solution containing 0.2 g of borax was gradually introduced and stirred thoroughly. Subsequently, 0.1 g of ammonium persulfate (APS) was added as an initiator, and the mixture was quickly homogenized and poured into a mold. The polymerization and gelation were carried out in a 50 °C oven for 1 hour to yield the final hydrogel sample (Fig. 1b).

The chemical structures of PVA, AM, and the resulting composite hydrogel were characterized by FTIR spectroscopy (Fig. 2a). In the spectrum of PVA, the broad absorption bands at 3425–3180 cm^{-1} are assigned to –OH stretching vibrations, while the peak at 1037 cm^{-1} corresponds to C–O stretching and the band at 1400 cm^{-1} is attributed to $-CH_2$ bending. For AM, the absorption band in the range of 3400–3190 cm^{-1} is assigned to N–H stretching, and the characteristic amide I and amide II bands appear at 1664 and 1453 cm^{-1}, respectively. In the spectrum of the composite hydrogel, these characteristic peaks become broadened or slightly shifted, especially in the –OH/–NH stretching region, suggesting the existence of intermolecular interactions, such as hydrogen bonding, between the PVA and PAAm components. In addition, the shift of the C–O-related peak from 1037 cm^{-1} to 1121 cm^{-1} is consistent

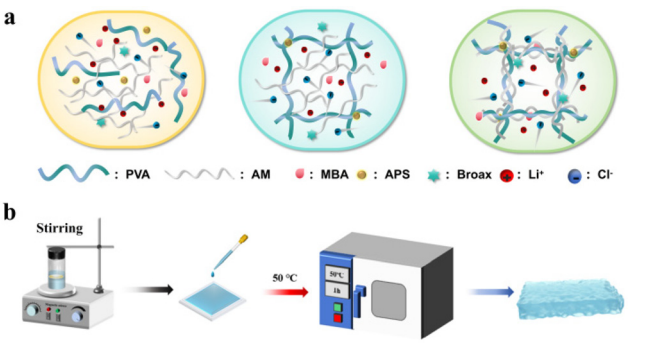

Fig. 1 (a) Schematic illustration of the dual-network crosslinking mechanism in the hydrogel. (b) Schematic representation of the hydrogel fabrication process.

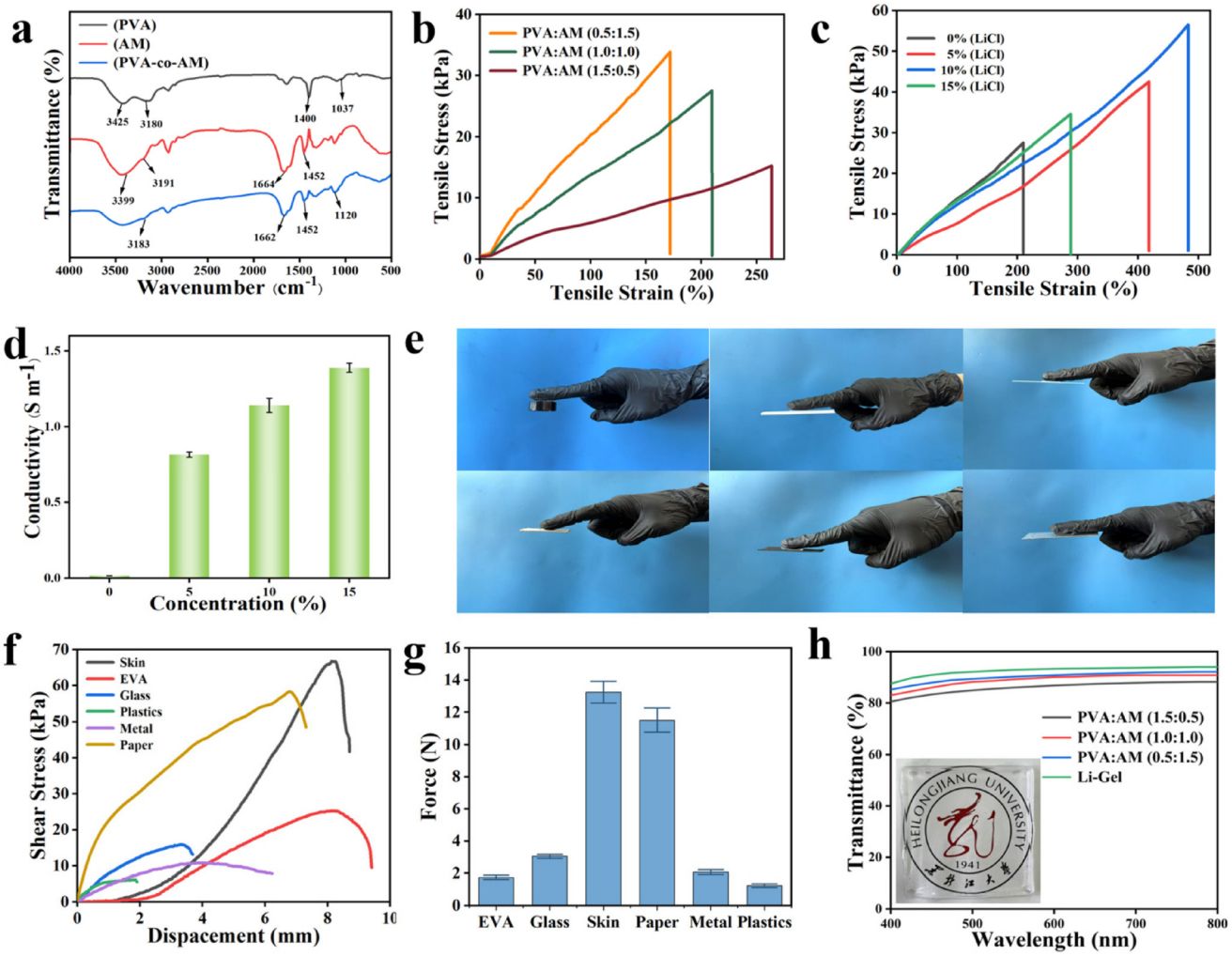

Fig. 2 (a) FTIR spectra of hydrogel samples; (b) stress–strain curves of PVA/PAAm hydrogels with different composition ratios; (c) mechanical properties of hydrogels after LiCl incorporation at various concentrations; (d) ionic conductivity of hydrogels with varying LiCl contents; (e) visual demonstration of hydrogel adhesion on various material surfaces; (f) lap shear test results showing adhesive strength of the hydrogel on different substrates; (g) statistical error bars of adhesive strength across various substrates; (h) side-view photographs showing visible light transmittance of different hydrogel films.

with a change in the local chemical environment of the PVA chains, which may be associated with borate–diol interactions. Overall, the FTIR results support the presence of intermolecular interactions in the hydrogel and are consistent with the proposed dual-network structure.

2.2. FTIR characterization and investigation of conductivity, adhesion, and light transmittance of hydrogels

In order to investigate the effect of the mass ratio of PVA to PAAm on the mechanical properties of the hydrogels, different ratios were designed in this study and the stress–strain curves were obtained by uniaxial tensile testing (Fig. 2b). The experimental results showed that the strain at break of the hydrogel increased significantly with the increase of PVA content. This is attributed to the flexible molecular chain structure of PVA and its formation of a reversible physical network, which effectively enhances the ductility of the material. However, the fracture stress decreased with increasing PVA percentage. This phenomenon may be related to the role of the PAAm network: the chemically crosslinked PAAm network provides the main mechanical support during the load-bearing process; when the PAAm content decreases, its crosslink density decreases, leading to a decrease in the overall strength.[17,18] Notably, when the mass ratio of PVA to PAAm was 1 : 1, the hydrogel achieved a good balance between strength and ductility and exhibited superior overall mechanical properties, indicating a significant synergistic effect between the two networks.

To improve the stability of PVA/PAAm dual-network hydrogels under low-temperature and drying conditions, various mass fractions of LiCl were introduced, and their effects on the mechanical properties were systematically investigated. As shown in Fig. 2c, when LiCl was not added, the strain at break of the hydrogel was about 200% and the ductility was moderate. When the LiCl content was increased to 10%, the tensile

properties of the hydrogel were significantly improved, and the strain at break increased to about 500%, indicating that an appropriate amount of LiCl can effectively improve the flexibility of the hydrogel. This performance enhancement mainly stems from the following mechanisms: the introduction of LiCl causes moderate swelling of the gel network, increasing the freedom of movement of the polymer chain segments, which facilitates the stretching and deformation of the network under external forces;[19] at the same time, there may be a certain degree of physical interactions between Li^+ and the functional groups on the polymer chains (*e.g.*, hydroxyl and amide groups), such as ion–dipole interactions, which enhance the reversible binding between the chain segments and synergistically improve the stress transduction. However, when the LiCl content was further increased to 15%, the mechanical properties of the hydrogels showed a decrease, and the fracture strain was significantly reduced. This may be attributed to the excessive swelling caused by the high concentration of LiCl, which weakened the interactions between the polymer chains, resulting in network loosening or even partial disintegration, ultimately reducing the overall mechanical strength of the material.[20]

The effect of LiCl concentration on the electrical conductivity of PVA/PAAm bi-network hydrogels was subsequently investigated. The experimental results showed that the introduction of LiCl significantly enhanced the ionic conductivity of the hydrogels (*e.g.*, Fig. 2d). When LiCl was not added, the initial conductivity of the hydrogel was low (about 0.01 S m^{-1}), which was difficult to meet the basic requirements for stable signal transmission in flexible electronic devices. With the increase of LiCl concentration, the hydrogel conductivity showed an increasing trend, and when the LiCl mass fraction was 10%, the conductivity was significantly increased to 1.1 S m^{-1}, an increase of two orders of magnitude. The significant improvement in the electrical conductivity mainly stems from the large number of freely migrating Li^+ and Cl^- ions generated by the dissociation of LiCl in the hydrogel network. These ions form effective continuous ion transport channels within the gel network, thereby substantially increasing the ion migration rate and overall electrical conductivity. In addition, the high conductivity helps to reduce the internal resistance of the gel and improve the stability and signal-to-noise ratio of signal transmission, making it more potential in application scenarios such as high frequency response and remote signal acquisition.[21] Taking into account the conductivity and mechanical properties (such as the aforementioned ductility optimization), 10% LiCl was identified as the optimal addition concentration. At this concentration, the hydrogel achieves both high ionic conductivity and excellent flexibility, demonstrating better overall performance. To simplify terminology in the following sections, the hydrogel containing the optimized concentration of LiCl is hereafter referred to as Li-Gel, while the formulation without LiCl is designated as P-Gel.

For conductive hydrogels intended for wearable human motion monitoring, stable adhesion to the skin and various material surfaces is essential to ensure reliable signal output.[22,23] Therefore, interfacial adhesion is regarded as a key parameter in evaluating their practical applicability. To assess the adhesive performance of Li-Gel, samples were applied to a range of common substrates, including glass, plastic (PMMA), paper, stainless steel, EVA foam, and porcine skin. As shown in Fig. 2e, Li-Gel adhered well to all tested surfaces without visible delamination or edge curling, indicating excellent conformability across diverse interfaces.

Quantitative evaluation of adhesion strength was performed using lap shear tests on a universal testing machine, and the average shear strength on each substrate was summarized in Fig. 2f. To ensure statistical accuracy, multiple parallel tests were conducted, and the results were presented as mean values with standard deviation error bars (Fig. 2g). The data revealed substrate-dependent variation in adhesion, with the highest adhesive force observed on porcine skin, reaching up to 13 N. This strong bio-adhesive property is likely due to the skin's microtextured surface and the presence of abundant polar functional groups, which can interact with the hydroxyl and amide groups in Li-Gel *via* hydrogen bonding and other non-covalent interactions, thereby enhancing interfacial bonding.

Transparency is one of the essential properties determining whether conductive hydrogels can enable intuitive visualization and information display in wearable sensors, electronic skin, and optical sensing devices.[24] In this study, the optical transmittance of PAAm-crosslinked PVA hydrogel films with varying ratios was evaluated in the visible range (400–800 nm) using a fluorescence spectrophotometer.

As shown in Fig. 2h, all prepared hydrogel films exhibited high transmittance, generally exceeding 80%, indicating good optical permeability of the hydrogel matrix. Notably, the transparency of Li-Gel was significantly enhanced, with the maximum transmittance reaching approximately 90%. This improvement can be attributed to two main factors: (1) the introduction of LiCl suppresses polymer chain aggregation, thereby reducing microscopic light-scattering sites and optical loss; and (2) Li^+ ions dynamically modulate the internal network structure, improving its uniformity and promoting consistent light transmission through the gel.

To visually demonstrate the optical transparency, hydrogel films were placed over standard printed patterns (*e.g.*, university logos) for qualitative assessment. The results showed that, regardless of LiCl addition, all films allowed clear pattern recognition, with well-defined edges and identifiable colors. In particular, the film containing 10% LiCl exhibited near-transparent behavior, producing minimal visual obstruction and confirming its excellent optical performance. In summary, Li-Gel not only maintains mechanical flexibility but also demonstrates outstanding visible light transmittance, underscoring its potential for integration into flexible sensors, display interfaces, and other smart wearable electronic applications.

2.3. Self-healing properties of hydrogels

While combining excellent mechanical and conductive properties, conductive hydrogels also rely heavily on self-healing

capabilities to ensure long-term operational stability in complex application environments. This is particularly critical in wearable devices and dynamic human–machine interfaces, where materials are frequently subjected to bending, stretching, and even mechanical damage.[25] Thus, imparting self-healing functionality is essential for extending device lifespan and maintaining continuous signal acquisition.[26]

To address this challenge, the present study employed the intrinsic dynamic crosslinking mechanism between polyvinyl alcohol (PVA) and borax to construct a dual-network conductive hydrogel—Li-Gel—with autonomous self-healing properties. Owing to the abundance of hydroxyl groups along PVA chains, dynamic borate ester bonds can reversibly form under the influence of borax, enabling the hydrogel to spontaneously reconstruct its network after mechanical disruption, without the need for external stimuli. This molecular-level repair mechanism is key to ensuring the material's long-term reliability.

A schematic illustration of this self-healing mechanism is presented in Fig. 3a. Upon recontact of the fractured surfaces, borate bonds between PVA chains are reformed, re-establishing the continuous hydrogel structure. Functional groups involved in the healing process are indicated with arrows, offering insight into the reversible interactions at play. Importantly, this self-healing process occurs without external triggers such as heat, moisture, or applied voltage, highlighting its practicality and adaptability to ambient conditions.

To investigate the microstructural recovery, scanning electron microscopy (SEM) was used to observe the cross-section of healed Li-Gel (Fig. 3b). The interface appeared smooth and integrated, with no discernible cracks or delamination, confirming successful rejoining of the polymer networks. Mechanical recovery was further evaluated through uniaxial tensile tests comparing pristine and self-healed samples (Fig. 3c). After 30 minutes of rest at room temperature, Li-Gel recovered approximately 80% of its original fracture strain and tensile strength, demonstrating substantial retention of mechanical performance. This restored extensibility and load-bearing capacity underscore the material's resilience and reusability in real-world applications.

To visually demonstrate interfacial repair, a color-contrast experiment was conducted (Fig. 3d). Two blocks of Li-Gel,

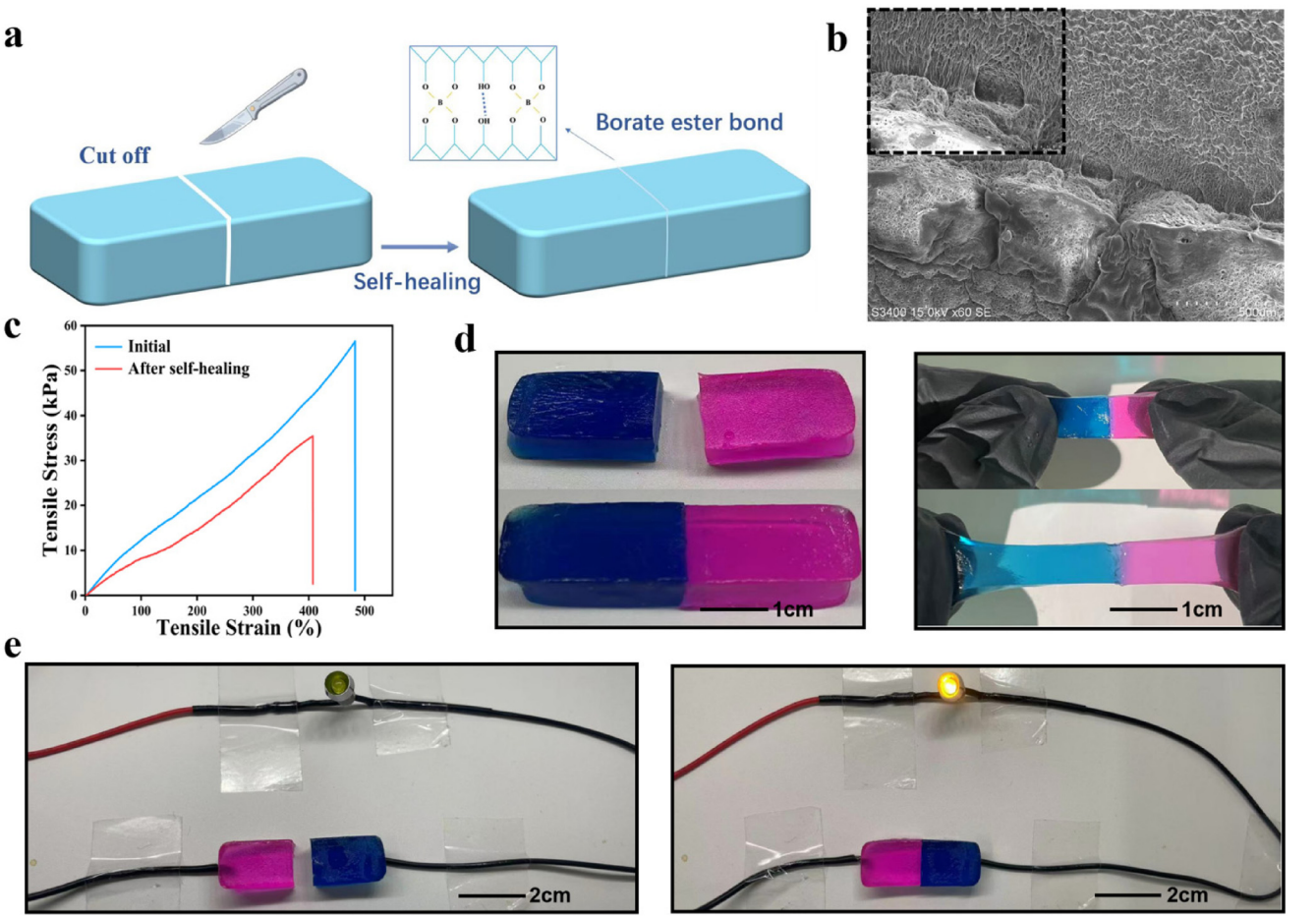

Fig. 3 (a) Schematic illustration of the self-healing mechanism in the hydrogel; (b) SEM image of the healed cross-section of the hydrogel; (c) photographs of tensile testing on pristine and self-healed hydrogels; (d) stress–strain curves comparing mechanical performance before and after healing; (e) electrical conductivity recovery test of the hydrogel after self-healing.

dyed with Rhodamine B (red) and methylene blue (blue), were cut and brought into contact. After 10 minutes, the healed sample was stretched without visible separation, confirming rapid and effective interfacial fusion. The distinct color contrast provides a clear visual indication of the healed interface, offering strong evidence of the material's rapid interfacial self-repair capability. In addition to structural restoration, functional recovery—specifically ionic conductivity—is critical for sensing applications. A closed-circuit test was performed (Fig. 3e), in which the colored segments of Li-Gel were connected in series with an LED *via* conductive wires. Upon healing, the LED illuminated successfully, indicating the reestablishment of ion transport pathways and restoration of electrical conductivity.

In summary, Li-Gel, based on dynamic and reversible borate crosslinking, exhibits excellent autonomous self-healing capability. It demonstrates not only efficient macro- and microstructural recovery but also substantial retention of mechanical strength and conductivity post-healing. The ability to self-repair without external intervention provides a robust foundation for long-term use in flexible and wearable electronic systems, including electronic skin and soft circuitry.

2.4. Water retention and anti-freezing properties of hydrogels

For conductive hydrogels intended for practical wearable sensing applications, long-term exposure to environmental stressors—such as air-drying, elevated temperatures, and subzero conditions—poses significant performance challenges.[27,28] Thus, evaluating a material's ability to retain mass and functional stability under ambient storage, thermal dehydration, and freezing environments is essential for determining its application reliability.

To systematically assess the environmental durability of the hydrogel developed in this study, three key tests were conducted: long-term water retention under ambient conditions, dehydration and subsequent mass recovery under high temperature, and antifreeze performance.

As shown in Fig. 4a, the long-term water retention behavior was evaluated under standard laboratory conditions (20 °C, 50% RH). Two colored samples were prepared: P-Gel (control, without LiCl) stained with Rhodamine B and Li-Gel (with LiCl) stained with methylene blue (representing the LiCl-doped formulation). After 7 days of ambient exposure, Li-Gel retained over 90% of its initial mass, while P-Gel experienced severe dehydration, maintaining less than 40% of its original weight. Corresponding optical images (Fig. 4b) showed that P-Gel exhibited visible shrinkage, surface whitening, and cracking, whereas Li-Gel remained soft, hydrated, and structurally intact.

These results highlight the superior water retention capability of Li-Gel, primarily attributed to the strong hydrophilicity of LiCl. Within the gel matrix, LiCl forms hydrated ionic clusters that tightly coordinate water molecules and lower the vapor pressure at the surface, thereby suppressing evaporation over time.

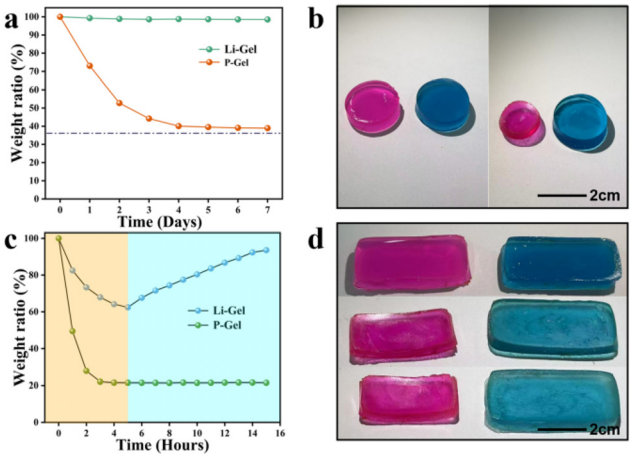

Fig. 4 (a) Comparison of mass retention between hydrogels with and without LiCl under ambient conditions; (b) photographs of hydrogel appearance after 7 days of exposure, with and without LiCl; (c) mass recovery performance of the hydrogel after thermal dehydration and ambient rehydration; (d) visual comparison of the hydrogel during high-temperature drying and post-rehydration recovery.

To further examine thermal tolerance, both Li-Gel and P-Gel were subjected to heating at 60 °C for 5 hours (Fig. 4c). After treatment, Li-Gel retained approximately 60% of its initial mass, while P-Gel dropped to about 20%, indicating extensive moisture loss. Upon returning to ambient conditions (20 °C, 55% RH) for 10 hours, Li-Gel showed strong mass recovery—exceeding 90% of its original weight—whereas P-Gel remained dried and brittle due to irreversible structural collapse.

A visual comparison of Li-Gel in its initial, dried, and rehydrated states is shown in Fig. 4d, demonstrating its robust moisture reabsorption capacity. This performance underscores the dual functionality of LiCl—not only as an ionic conductor but also as a hydration regulator.[29] During dehydration, LiCl contributes to a highly hydrated microenvironment, effectively acting as an internal "ionic reservoir" that delays total water loss. Moreover, its strong osmotic potential promotes the absorption of ambient moisture, enabling the hydrogel to autonomously rehydrate—a form of "self-regeneration". This property is especially beneficial for wearable sensors operating in fluctuating environments—such as prolonged outdoor exposure or repeated drying-rehydration cycles—by providing improved durability and consistent signal performance over time.

To evaluate the antifreeze properties of the hydrogel under subzero conditions, differential scanning calorimetry (DSC) was conducted on Li-Gel, and the results are presented in Fig. 5a. A distinct exothermic peak, corresponding to the freezing transition was observed at −13.5 °C, significantly lower than the freezing point of pure water. This marked depression in freezing temperature is attributed to the presence of LiCl, which disrupts the hydrogen bonding network essential for ice nucleation and crystal growth.[30] By interfering with the ordering of water molecules, LiCl effectively

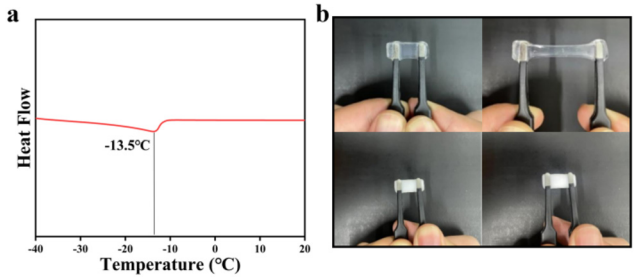

Fig. 5 (a) Differential scanning calorimetry (DSC) analysis of the hydrogel to assess its antifreeze performance; (b) visual comparison of flexibility between hydrogels with and without LiCl at 0 °C.

inhibits ice formation, allowing the hydrogel to remain in a non-frozen state even below 0 °C.

The macroscopic antifreeze behavior of Li-Gel was further confirmed by comparing Li-Gel with P-Gel at 0 °C (Fig. 5b). While Li-Gel remained transparent, flexible, and free of visible crystallization or whitening, P-Gel froze rapidly, turning opaque and rigid with a white appearance—clear signs of ice formation and mechanical failure. These results underscore the importance of the stable hydration shells formed through ionic interactions between Li^+ ions and water molecules, which serve to suppress freezing and preserve flexibility.

This mechanism ensures that Li-Gel maintains its structural integrity and functional performance in cold environments, highlighting its potential for wearable sensing applications in subzero or outdoor conditions where conventional hydrogels would otherwise fail.

2.5. Sensor-oriented testing and application of hydrogels

The conductivity of Li-Gel primarily originates from the migration of mobile ions within its polymeric network. When subjected to external mechanical deformation such as stretching or compression, the internal microstructure undergoes changes that affect ion migration pathways, concentration gradients, and interfacial resistance—resulting in measurable electrical resistance fluctuations. This forms the basis for real-time strain sensing. In Li-Gel, a LiCl-mediated ionic conduction mechanism enables the formation of a stable and continuous ion-transport network. Due to the high solubility and rapid mobility of Li^+ and Cl^- ions, the hydrogel responds rapidly to mechanical stimuli, conferring excellent strain-sensing capability.

To comprehensively evaluate the sensing performance of Li-Gel under diverse mechanical conditions, a series of tests were conducted, including strain sensitivity, dynamic stability, response time, frequency response, and cyclic durability. As shown in Fig. 6a, the relative resistance change ($\Delta R/R_0$) was

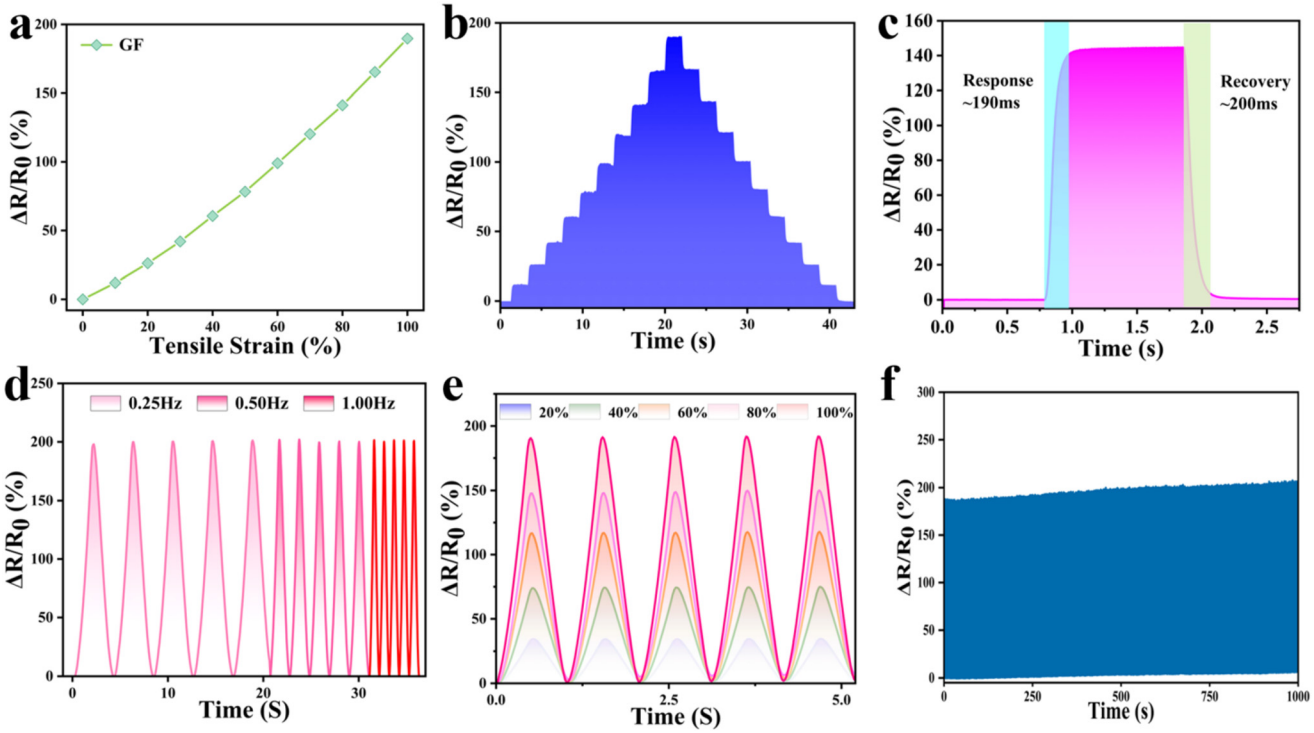

Fig. 6 (a) Relative resistance variation ($\Delta R/R_0$) of Li-Gel under tensile deformation, indicating its strain sensitivity. (b) Stepwise stretching and releasing cycle used to evaluate the hydrogel's response stability under progressive mechanical input. (c) Rapid electrical response of Li-Gel under sudden 100% strain, demonstrating its fast sensing dynamics. (d) Real-time resistance waveforms under stretching frequencies of 0.25 Hz, 0.5 Hz, and 1.0 Hz, validating frequency adaptability. (e) Electrical signal outputs under different strain amplitudes, confirming consistent and repeatable sensing performance. (f) Long-term durability test over 1000 stretching cycles at 100% strain, verifying the hydrogel's mechanical resilience and sensing repeatability.

recorded under incremental tensile strain, and the gauge factor (GF) was calculated. At 100% strain, Li-Gel exhibited a GF of 2.00, indicating a reliable and nearly linear strain response to deformation. This value compares favorably with typical ionic conductive hydrogels, suggesting its suitability for detecting moderate physiological movements such as joint bending and muscle contraction.

To assess the material's consistency under cyclic loading and unloading, a "pyramid-shaped" stepwise strain test was carried out (Fig. 6b). The hydrogel was stretched incrementally from 10% to 100% in 10% steps at 2-second intervals, followed by symmetric unloading at the same rate. The resulting resistance–time curve showed clear, well-defined stepwise changes with sharp transitions, demonstrating excellent signal fidelity, controllability, and structural integrity without observable lag or drift. This suggests that Li-Gel maintains stable conductive pathways with rapid reconstruction during mechanical cycling.

The instantaneous response capability of Li-Gel was further examined under sudden deformation at 100% strain (Fig. 6c). The response time was found to be under 200 ms, indicating that the ion-conducting network can rapidly adapt to transient mechanical perturbations. This fast response is particularly valuable for detecting quick motions such as facial expressions, finger gestures, or speech-induced strain.

To evaluate performance under varying actuation rates, stretching tests were performed at frequencies of 0.25 Hz, 0.5 Hz, and 1.0 Hz (Fig. 6d). In all cases, Li-Gel produced periodic, amplitude-stable signal waveforms without distortion or drift, confirming reliable structural periodicity and conductive network resilience under dynamic conditions.

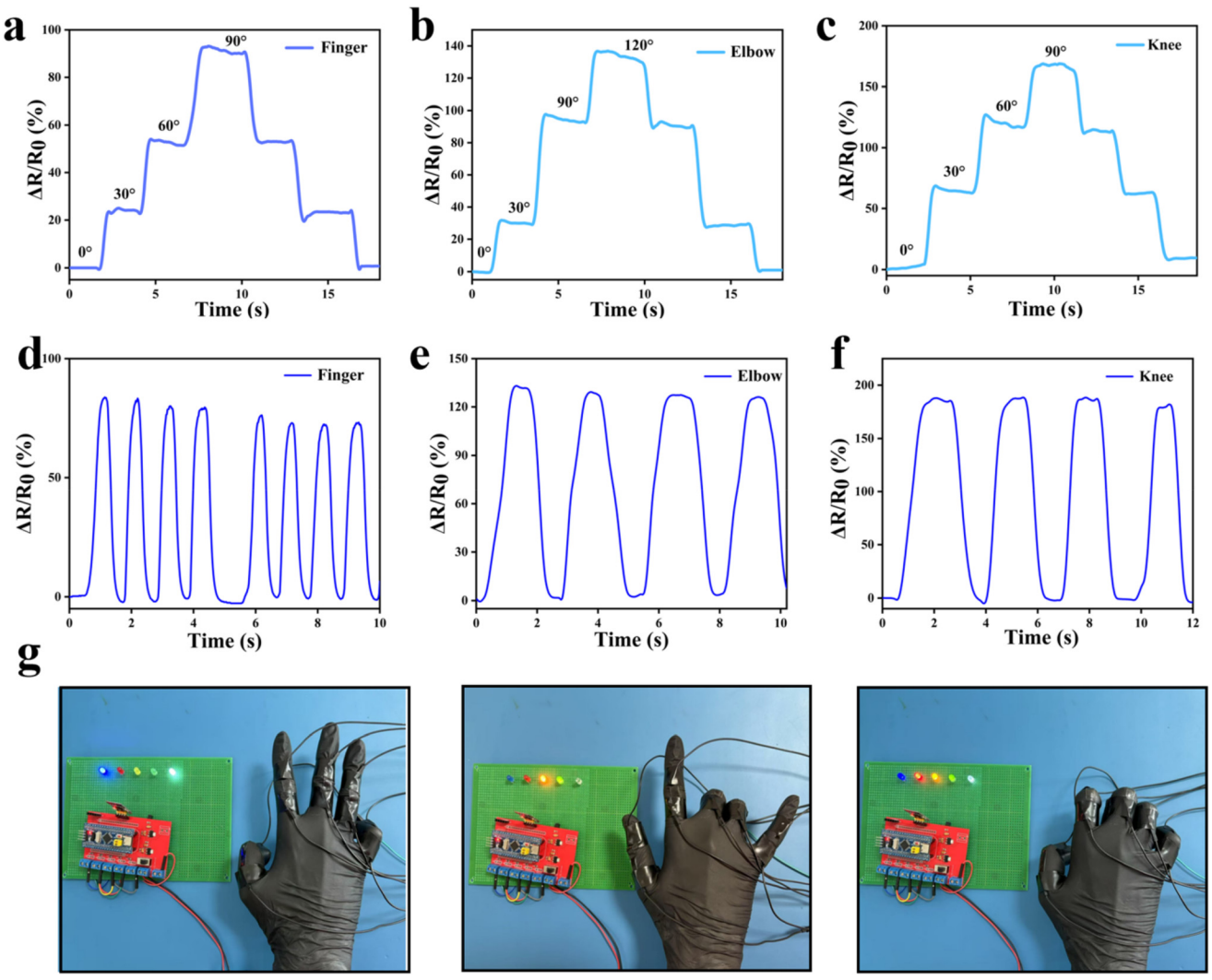

Fig. 7 (a–c) Real-time electrical signal responses of Li-Gel adhered to the finger, elbow, and knee during different degrees of bending motion. (d–f) Electrical stability of Li-Gel under repeated bending–releasing cycles at the same anatomical locations: finger, elbow, and knee, respectively. (g) Schematic illustration of Li-Gel functioning as a wearable strain sensor to control LED switching, demonstrating its application in motion-triggered electronic control systems.

To investigate its performance across different strain magnitudes, cyclic tests were performed at 20%, 40%, 60%, 80%, and 100% strain levels (Fig. 6e). The resistance signals remained consistent in each case, indicating robust sensing accuracy over a wide strain range. Finally, to assess long-term durability, Li-Gel was subjected to 1000 consecutive stretch–release cycles (Fig. 6f). Throughout the test, the GF remained stable at 2.00, with no signal attenuation or performance degradation, confirming exceptional fatigue resistance and structural recovery.

In summary, Li-Gel demonstrates reliable sensing characteristics, including a reproducible strain response, rapid response time, frequency stability, and long-cycle durability. These attributes support its applicability in flexible strain sensing for motion tracking, health monitoring, and human–machine interaction.

To further demonstrate the practical applicability of the developed conductive hydrogel (Li-Gel) in wearable systems, we systematically evaluated its performance in human motion monitoring and signal-driven electronic control. Owing to its excellent flexibility, adhesion, and electrical responsiveness,[31] Li-Gel stably conforms to skin surfaces and reliably detects strain associated with joint movements. As shown in Fig. 7a–c, Li-Gel was attached to representative joints including the fingers, elbows, and knees to monitor natural bending and extension. Joint movements induced mechanical deformation in the hydrogel, triggering internal ionic migration and resulting in stable, distinguishable changes in resistance. The resulting electrical signals exhibited clear waveform boundaries, symmetric responses, and high repeatability, confirming the material's ability to deliver high-quality sensing output under multi-site attachment.

To assess the stability of Li-Gel under dynamic operating conditions, repeated bending–releasing cycles were performed on the same joints (Fig. 7d–f). Even after continuous strain cycles, the sensing signals remained highly consistent without evident drift or degradation, indicating strong structural resilience and signal durability under repetitive mechanical stress. These results confirm that Li-Gel meets the high-frequency operational requirements of wearable sensors in daily activity monitoring.

Beyond basic motion sensing, Li-Gel also exhibited strong potential for signal output and system integration. By interfacing the hydrogel with a microcontroller unit (MCU), a flexible signal control platform was established. In this setup, body movements induced by Li-Gel deformation generated graded electrical outputs that were used to drive an LED through three distinct states: on, blinking, and off. This illustrates the material's capability to bridge physical stimuli and active behavioral control. Furthermore, a multi-point input encoding strategy was implemented, wherein five individual Li-Gel patches were affixed to each finger, enabling discrete strain signals from each digit. By combining different activation patterns, the system achieved 243 distinct signal combinations (3^5 encoding), supporting high-density information input and gesture-based command recognition.

These findings highlight Li-Gel's versatility in multi-channel motion sensing and composite signal output, underscoring its potential in information encoding, wearable electronics, and human–machine interaction. Overall, the successful demonstration of Li-Gel in real-world joint monitoring and multi-level signal control validates its transition from a flexible sensing material to an integrated system component, offering a viable material platform for next-generation wearable devices with high sensitivity, environmental adaptability, and input/output scalability.

3. Conclusions

In summary, a multifunctional conductive hydrogel (Li-Gel) was developed based on a dual-network architecture of PVA and PAAm, dynamically crosslinked *via* borate interactions and ionically modified with LiCl. The resulting material exhibits excellent mechanical flexibility, reliable ionic conductivity (~1.1 S m^{-1}), and robust performance under mechanical strain, making it well-suited for strain-sensing applications. Notably, Li-Gel maintains high electrical responsiveness even under repeated deformation, demonstrating fast response times (<200 ms), stable signal output across various frequencies and strain levels, and no significant degradation after 1000 cycles. Beyond its mechanical and electrical properties, Li-Gel also exhibits good environmental adaptability. Owing to the incorporation of LiCl, the hydrogel shows enhanced water retention and self-rehydration capability under ambient and elevated-temperature conditions, which supports its long-term stability during use. This self-regeneration behavior, combined with its self-healing capacity, ensures signal continuity and material stability in complex, real-world environments. These findings indicate that Li-Gel provides a multifunctional and practically relevant hydrogel design for wearable sensing applications requiring mechanical adaptability, environmental tolerance, and stable signal output.

Author contributions

Zhongyuan Lin: conceptualization, methodology, investigation, formal analysis, writing – original draft, writing – review editing. Ze Li: software, validation, investigation, resources, data curation, writing – review & editing. Xinpeng Lv: methodology, validation, investigation, data curation, visualization, writing – review & editing. Yuhang Shen: investigation, resources, data curation. Chunpeng Ai: supervision, project administration, funding acquisition, resources, writing – review & editing. Peng Li: supervision, funding acquisition, writing – review & editing.

Conflicts of interest

There are no conflicts to declare.

Data availability

The original data supporting the findings of this study are available upon reasonable request from the corresponding author.

Acknowledgements

The authors acknowledge the financial support from the 2024 Supervision of the New Round of Heilongjiang Provincial "Double First-Class" Disciplines Collaborative Innovation Achievement Project (Grant No. LJGXCG2024-P18) and Program for Young Talents of Basic Research in Universities of Heilongjiang Province (YQJH2024196).

References

1 X. Han, X. Qiu, M. Zong and J. Hao, *Small Struct.*, 2023, **4**, 2300090.
2 Z. Liu, Y. Wang, Y. Ren, G. Jin, C. Zhang, W. Chen and F. Yan, *Mater. Horiz.*, 2020, **7**, 919–927.
3 H. Zhang, H. Shen, J. Lan, H. Wu, L. Wang and J. Zhou, *Carbohydr. Polym.*, 2022, **295**, 119848.
4 X. Li, S. Zhang, X. Li, L. Lu, B. Cui, C. Yuan, L. Guo, B. Yu and Q. Chai, *Carbohydr. Polym.*, 2023, **320**, 121262.
5 Y. Ma, D. Zhang, Z. Wang, H. Zhang, H. Xia, R. Mao, H. Cai and H. Luan, *ACS Appl. Mater. Interfaces*, 2023, **15**, 29413–29424.
6 H. Zhang, W. Niu and S. Zhang, *ACS Appl. Mater. Interfaces*, 2019, **11**, 24639–24647.
7 Y. Ni, X. Zang, J. Chen, T. Zhu, Y. Yang, J. Huang, W. Cai and Y. Lai, *Adv. Funct. Mater.*, 2023, **33**, 2301127.
8 X. Peng, W. Wang, W. Yang, J. Chen, Q. Peng, T. Wang, D. Yang, J. Wang, H. Zhang and H. Zeng, *J. Colloid Interface Sci.*, 2022, **618**, 111–120.
9 Q. Xu, M. Hou, L. Wang, X. Zhang and L. Liu, *Chem. Eng. J.*, 2023, **477**, 147065.
10 Y. Jian, B. Wu, X. Le, Y. Liang, Y. Zhang, D. Zhang, L. Zhang, W. Lu, J. Zhang and T. Chen, *Research*, 2019, **2019**, 2384347.
11 X. Gong, C. Zhao, Y. Wang, Y. Luo and C. Zhang, *ACS Biomater. Sci. Eng.*, 2022, **8**, 3633–3643.
12 R. Liu, Y. Liu, S. Fu, Y. Cheng, K. Jin, J. Ma, Y. Wan and Y. Tian, *Small*, 2024, **20**, 2308092.
13 B. Guo, M. Yao, S. Chen, Q. Yu, L. Liang, C. Yu, M. Liu, H. Hao, H. Zhang, F. Yao and J. Li, *Adv. Funct. Mater.*, 2024, **34**, 2315656.
14 C. He, S. Bi, R. Liu, H. Zhao, C. Chen, X. Zhao, J. Gu and B. Yan, *ACS Appl. Mater. Interfaces*, 2024, **16**, 35887–35897.
15 C. Cai, C. Wen, W. Zhao, S. Tian, Y. Long, X. Zhang, X. Sui, L. Zhang and J. Yang, *ACS Appl. Mater. Interfaces*, 2022, **14**, 23692–23700.
16 X. Li, M. Jiang, Y. Du, X. Ding, C. Xiao, Y. Wang, Y. Yang, Y. Zhuo, K. Zheng, X. Liu, L. Chen, Y. Gong, X. Tian and X. Zhang, *Mater. Horiz.*, 2023, **10**, 2945–2957.
17 H. Zhang, J. Guo, Y. Wang, L. Sun and Y. Zhao, *Adv. Sci.*, 2021, **8**, 2102156.
18 J. Shen, L. Lu, R. He, Q. Ye, C. Yuan, L. Guo, M. Zhao and B. Cui, *Carbohydr. Polym.*, 2024, **346**, 122608.
19 Z. Yang, D. Shi, W. Dong and M. Chen, *Chem. – Eur. J.*, 2020, **26**, 1846–1855.
20 X. Yao, H. Chen, H. Qin, Q.-H. Wu, H.-P. Cong and S.-H. Yu, *Nat. Commun.*, 2024, **15**, 9254.
21 H. Wang, Q. Ding, Y. Luo, Z. Wu, J. Yu, H. Chen, Y. Zhou, H. Zhang, K. Tao, X. Chen, J. Fu and J. Wu, *Adv. Mater.*, 2023, **36**, 2309868.
22 Y. Xu, Z. Sun, Z. Bai, H. Shen, R. Wen, F. Wang, G. Xu and C. Lee, *Nat. Commun.*, 2024, **15**, 6022.
23 J. Wu, J. Xian, C. He, H. Lin, J. Li and F. Li, *Adv. Mater.*, 2024, **36**, 2405372.
24 Z.-L. Wang, Z.-P. Deng, F. Wang, X.-L. Wang, Y.-Z. Wang and F. Song, *Chem. Eng. J.*, 2023, **478**, 147364.
25 X. Yan, Q. Chen, L. Zhu, H. Chen, D. Wei, F. Chen, Z. Tang, J. Yang and J. Zheng, *J. Mater. Chem. B*, 2017, **5**, 7683–7691.
26 J. Wu, Z. Wu, X. Lu, S. Han, B.-R. Yang, X. Gui, K. Tao, J. Miao and C. Liu, *ACS Appl. Mater. Interfaces*, 2019, **11**, 9405–9414.
27 X. Deng, W. Wang, D. Du and C. Luo, *ACS Appl. Polym. Mater.*, 2023, **5**, 6346–6353.
28 W. Peng, X. Pan, X. Liu, Y. Gao, T. Lu, J. Li, M. Xu and L. Pan, *J. Colloid Interface Sci.*, 2023, **634**, 782–792.
29 Z. Xu, F. Zhou, H. Yan, G. Gao, H. Li, R. Li and T. Chen, *Nano Energy*, 2021, **90**, 106614.
30 Y. Zhang, T. Li, L. Miao, P. Kaur, S. Men, Q. Wang, X. Gong, Y. Fang, C. Zhai, S. Zhang, L. Zhang and L. Ye, *J. Mater. Chem. A*, 2022, **10**, 3970–3988.
31 K. Chen, K. Liang, H. Liu, R. Liu, Y. Liu, S. Zeng and Y. Tian, *Nano-Micro Lett.*, 2023, **15**, 102.